Energy & Environmental Science

PAPER

View Article Online
View Journal

Cite this: DOI: 10.1039/c5ee01705j

Mesoporous pores impregnated with Au nanoparticles as effective dielectrics for enhancing triboelectric nanogenerator performance in harsh environments†

Jinsung Chun,[a] Jin Woong Kim,[a] Woo-suk Jung,[b] Chong-Yun Kang,[c] Sang-Woo Kim,[d] Zhong Lin Wang[e] and Jeong Min Baik*[a]

Received 1st June 2015,
Accepted 6th August 2015

DOI: 10.1039/c5ee01705j

www.rsc.org/ees

A facile and scalable synthesis of mesoporous films impregnated with Au nanoparticles (NPs) as effective dielectrics is demonstrated for enhancing the nanogenerator performance based on vertical contact-separation mode. This technique is so simple and scalable, providing a promising solution for developing large-scale and practical self-powered devices. The spatial distribution of Au NPs made it possible to fabricate an Au NP-embedded mesoporous triboelectric nanogenerator (AMTENG) with a high output power of 13 mW under cycled compressive force, giving over 5-fold power enhancement, compared with a flat film-based TENG under the same mechanical force. It is proposed that the presence of aligned dipoles produced due to the charges created by the contact between Au NPs and PDMS inside the pores can influence the surface potential energy of mesoporous films. With such an enhanced power output and unique device design, we demonstrate various applications such as self-powered shape mapping sensors, foot-step driven large-scale AMTENGs, and integrated circuits with capacitors for powering commercial cell phones for realizing self-powered systems from footsteps, wind power, and ocean waves.

Broader context

Triboelectric nanogenerators (TENGs) are a new class of power generating devices that can effectively convert ambient mechanical energy into electricity, based on triboelectric effects coupled with electrostatic effects. So far, interesting material modifications, such as the dielectric constant, compressibility, and the surface potential, in a few types of TENGs have been reported for high output performance of TENGs. However, the surface charge density was primarily determined by the intrinsic properties of the specific materials and there are no effective ways to enhance the output power of TENGs. Here, we report a facile and scalable synthesis of mesoporous films impregnated with Au nanoparticles as effective dielectrics for enhancing the TENG's performance. This technique is so simple and scalable, providing a promising solution for developing large-scale and practical self-powered devices. The nanogenerator shows the instantaneous power of 13 mW, giving over 5-fold power enhancement, compared with a flat film-based nanogenerator due to the aligned dipoles produced by the charges created by the contact between Au NPs and PDMS inside the pores. Our results will lead to the further advancement of nanogenerators as promising large-scale power supplies for realizing self-powered systems from footsteps, wind power, and ocean waves.

1. Introduction

Mechanical energy is one of the most ubiquitous energies in our surroundings, which can be converted into electricity at anytime and anywhere.[1–5] Since 2012, a power generating device, named as the triboelectric nanogenerator (TENG), has been proven as cost effective, simple, and efficient techniques for energy harvesting.[6–20] Until now, various applications of TENGs have been successfully demonstrated, such as self-powered sensors,[7] self-charging cells,[8] trace memory systems,[21] distress signal emitters,[22] and self-electroplating technology.[23]

In the TENGs, surface charge transfer is achieved between two materials that are in physical contact.[24] The subsequent separation of the two charged materials induces an electronic potential difference, driving the flow of electrons through an external load.[9] In traditional TENGs, the two materials were chosen according to the difference in surface potentials, *e.g.*, the polymer material (*i.e.* Teflon)[25] terminated with the most electronegative functional group as the negative side and the

[a] School of Materials Science and Engineering, KIST-UNIST-Ulsan Center for Convergent Materials, Ulsan National Institute of Science and Technology (UNIST), Ulsan, 689-798, Republic of Korea. E-mail: jbaik@unist.ac.kr
[b] Electronic Materials Research Center, Korea Institute of Science and Technology (KIST), Seoul, 137-791, Republic of Korea
[c] KU-KIST Graduate School of Converging Science and Technology, Korea University, Seoul, 136-701, Republic of Korea
[d] School of Advanced Materials Science and Engineering, Sungkyunkwan University (SKKU), Suwon, 440-746, Republic of Korea
[e] School of Materials Science and Engineering, Georgia Institute of Technology, Atlanta, Georgia 30332-0245, USA

† Electronic supplementary information (ESI) available. See DOI: 10.1039/c5ee01705j

low work function material (*i.e.* Al metal)[26] as the positive side, apart from each other (named airgap). In physical contact, the polymer at the negative side gains electrons from Al, being negative compared with Al. Thus, a key approach to improve the output performance of the TENGs from the material aspect is to increase the triboelectric surface charge density through material modification and surface functionalization.[27] So far, interesting material modifications such as the dielectric constant,[28] compressibility,[7,29] and the surface potential,[30] in a few types of TENG have been reported. However, the density of surface charges was primary determined by the intrinsic properties of the specific materials and there are no effective ways to enhance the output power of TENGs.

In this work, we report a facile and scalable synthesis of mesoporous films impregnated with Au nanoparticles (NPs) as effective dielectrics for enhancing the TENG's performance based on vertical contact-separation mode. Bulky and mesoporous polydimethylsiloxane (PDMS) film was fabricated by casting a mixture of PDMS solution and DI water, evaporating water very slowly at room temperature. Before making the mixture of the PDMS solution and DI water, Au NPs were introduced into DI water. After the subsequent evaporation process of water, we found that the Au NPs were accumulated only at the bottom side of the pores. This technique is very simple and scalable, providing a promising solution for developing large-scale and practical self-powered devices. The spatial distribution of the Au NPs made it possible to fabricate an Au NP-embedded mesoporous TENG (AMTENG) with a high output power density of 13 mW (160 $\mu W\ cm^{-2}$) under cycled compressive force, giving over 5-fold power enhancement, compared with a flat film-based TENG (FTENG) under the same mechanical force. It is proposed that the presence of aligned dipoles produced due to the charges created by the contact between Au NPs and PDMS inside the pores can influence the surface potential energy of mesoporous films. The electrical output performance of the AMTENG was measured under several mechanical stresses. Various AMTENGs were fabricated using different porosities of the mesoporous structures and different Au concentrations inside pores. With such an enhanced power output and unique device design, we demonstrate various applications such as self-powered shape mapping sensors, foot-step driven large-scale AMTENGs, and integrated circuits with capacitors for powering commercial cell phones.

2. Experimental section

Polydimethylsiloxane (PDMS) (Sylgard 184, Dow Corning), which was used as the polymer layer with many pores, was prepared by the gel-casting technique. A solution of mixed base monomers and the curing agent in a mass ratio of 10 : 1 was added to a beaker. The air remaining in PDMS was removed by a vacuum process and PDMS was mixed with deionized (DI) water. The mass ratio between DI water to PDMS was adjusted to create different porosities. The mixture was stirred for 30 min and yielded a uniformly-mixed PDMS/DI water suspension. The suspension was cast into a film shape in a blocking layer on an SiO_2/Si substrate and dried in atmosphere at 90 °C to remove DI water and create air voids in PDMS. After the PDMS film layer was peeled off from the substrate, a mesoporous structured PDMS film was obtained. To position Au NPs on the bottom side of pores in the mesoporous film, the mesoporous film was dipped into the 100 nm colloidal Au suspension (BBI International, UK) for 5 h and then taken out. After cleaning the surface of the film with DI water, the mesoporous film with Au NPs and DI water was then dried slowly in atmosphere at room temperature for 72 h to remove DI water. This slow drying process is very important so that the nanoparticles are located at the bottom side of the pores (Fig. S1, ESI†). To fabricate the nanogenerator, a 10 μm-thick PDMS film was produced on the Al electrode attached by the double sided polyimide tape, as shown in the schematic fabrication process of the TENG (Fig. S2a, ESI†). The mesoporous PDMS film was then attached on the layer and covered with the same PDMS film/polyimide/Al electrode, followed by drying in atmosphere at 90 °C for 1 h. In the cross sectional optical and SEM images, it was found that there was no gap between these layers (Fig. S2b, ESI†).

We measured the output voltage and current density of the AMTENG under a vertical compressive stress using an Agilent Technologies DSO 1204A oscilloscope and low-noise current preamplifier (model no. SR570, Stanford Research Systems, Inc.). The transferred charge density from the output signals was measured using a Keithley 6514 system electrometer. A pushing tester (Labworks Inc., model no. ET-126-4) was used to apply the vertical force to the nanogenerator.

The morphologies of the fabricated mesoporous films were investigated by using a Nano 230 field emission scanning electron microscope (FEI, USA). Compression tests were carried out under a maximum stress of 30 N using a Mecmesin Multitest i-1 (Slinfold, United Kingdom).

A home-made apparatus was employed to examine the effect of humidity on the output current density of the generators. The humid air from a humidifier, balanced by dry air, was introduced into the chamber under 1 atm of a dry air background. By controlling the valve between the humid/air sources, the humidity inside the chamber can be either increased or decreased, in the range of 20 to 95%, measured using a humidity sensor (Daekwang Instrument Inc., TH-05, Republic of Korea). The nanogenerators were then placed in the chamber and the output signals were measured with the relative humidity as a function of holding time (5 min).

3. Results and discussion

A schematic diagram representing the fabrication of the AMTENG and the resulting free-standing mesoporous film is shown in Fig. 1a. The scanning electron microscopy (SEM) images in Fig. 1b show the sponge-like mesoporous structures of the PDMS film after removal of DI water and Au NPs inside the pores. PDMS is inherently hydrophobic, thus, the water in the PDMS solution attempts to form a spherical shape in the PDMS/DI water mixture. As pore initiation is random, the pores

with a broad size distribution are randomly arranged. However, this approach is an easy fabrication method of scalable nanogenerators based on sponge-like mesoporous films for developing practical self-powered electronic systems. The porosity increases to approximately 59% as the amount of water increases to 50%, as shown in Fig. 1c, To calculate the porosity of the mesoporous film, the SEM images in the inset of Fig. 1c were first converted into binary images, and the MATLAB image processing toolbox was used to sum total the volume of pores in the film.[31] The porosity (V_{pore}/V_{total}) was calculated by dividing the volume of pores formed in the mesoporous film by the total volume of film. Using this method, a large-area mesoporous PDMS thin film (30 cm × 30 cm) was fabricated (Fig. 1d), demonstrating the capability of producing large-scale films. The photograph in the inset of Fig. 1d and the movie in the ESI,† Fig. S3, representing a manual compression test of the mesoporous film with a volume reduction of over 50%, show that the as-fabricated thin film almost perfectly recovers its original shape after the release of the compressive force, remarkably compliant and springy. To measure the compressibility of the mesoporous films with porosities from 0 to 59% and evaluate resistance to deformation by external forces, compressibility measurements were conducted on the films, as shown in Fig. 1e. Fig. 1e shows the loading and unloading stress–strain curves for mesoporous films with porosities from 0 to 59%. It is obvious that the loading and unloading curves for all samples are almost identical. This indicates that plastic collapse in the mesoporous films does not occur during loading and unloading. As the porosity increases, it is clearly seen that the elastic modulus decreases, thereby, the mesoporous film becomes more flexible.

The TENG based on the mesoporous film was fabricated by attaching metal electrodes (Al foil in our case) to both sides of the film. Most of the TENGs have an airgap between a polymer film and a metal electrode, which not only helps in successive contact and separation, but also affects the electrical potential and charge density. The gap distance, which varies considerably from 1 to 3 mm,[8,27] significantly affects the electrical output performance of the device. Without an airgap, a very poor electrical output performance was seen in TENGs.[6] However, the presence of the gap may require a complicated fabrication effort and may limit the large-scale fabrication of practical devices. More importantly, an airgap left between the two layers makes such devices sensitive to moisture, and their packaging becomes a major issue. This strongly limits their applications in liquids.

Fig. 2a and b show the output voltage and output current density of the AMTENG without an airgap as a function of the Au content (in weight percent) ranging from 0.058 to 0.28 wt% in the pores, measured under a cycled compressive force of around 90 N at an applied frequency of 5 Hz. As expected, the PDMS thin film shows a poor AC-type electrical output performance of less than approximately 5 V and 0.006 μA cm^{-2}. This small output signal may be attributed to the presence of small gaps at the interface between the layers. Actually, we fabricated various TENGs with gaps between the PDMS and Al layers from 0.1 to 0.5 mm and their output performance was plotted in Fig. S4 (ESI†). The results show that the small outputs may have

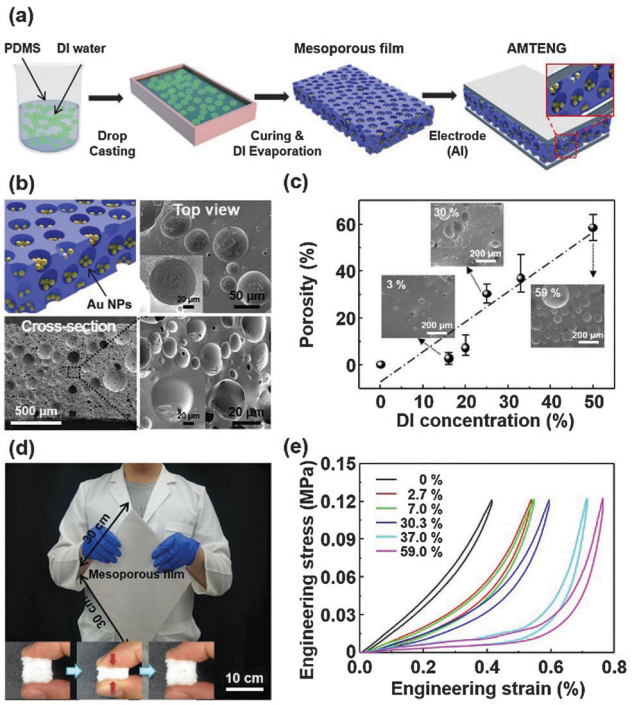

Fig. 1 (a) Schematic diagrams of the fabrication process for the AMTENG. (b) Top and cross-sectional SEM images of a mesoporous PDMS film with Au NPs (0.28 wt%). The insets show the morphology of Au NPs and cross-sectional SEM images of the mesoporous film. (c) Porosity changes as a function of the DI water concentration ranging from 0 to 50%. The insets show SEM images of mesoporous films with various porosities. (d) Photographs of a fabricated large-area mesoporous PDMS thin film (30 cm × 30 cm). The insets show manual compression with a volume reduction of over 50%. (e) The loading and unloading stress–strain curves as a function of the porosity ranging from 0 to 59%.

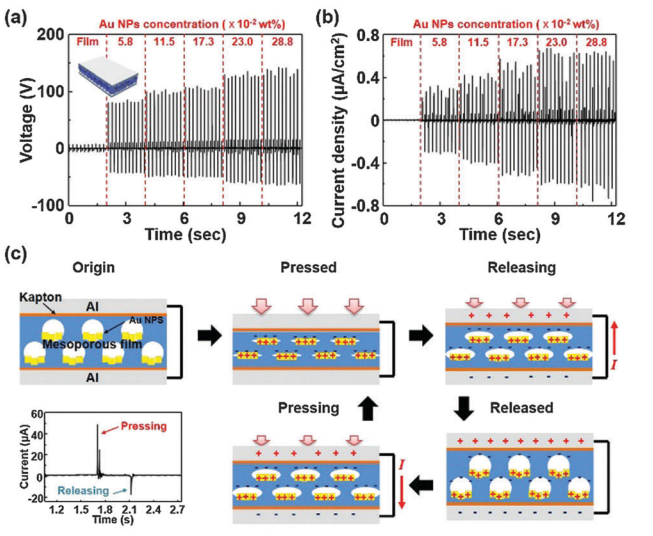

Fig. 2 (a) The output voltage and (b) current generated by the AMTENG as a function of the Au NP concentration ranging from 5.8 to 28.8 × 10^{-2} wt%. (c) The charge generation mechanism of the AMTENG under an external force and short-circuit conditions.

originated from some small gaps, however, the gaps (if any) should be very small, less than 100 μm. It is obvious that as the Au content increases to 0.28 wt%, the output voltage and current density reach 150 V and 0.62 μA cm^{-2} under the same mechanical force, much larger than that of the film-type generator.

Under open-circuit conditions, the charge generation of the AMTENG under cycled compressive force can be understood from the coupling of the triboelectric effect and electrostatic induction. Before the contact of Au NPs and the PDMS inside pores, there is no charge transfer, and thus no potential generated. By the compressive force, friction between two materials occurs and electrons are transferred from Au NPs to PDMS film, resulting in positive and negative charges on both surface. As the force is withdrawn, the contacting surfaces are separated (Fig. S5, ESI†). Based on the above mechanism, the output voltage is usually shown as a direct current (DC) signal. However, the AMTENG shows a sharp alternating current (AC) signal in Fig. 2a. This may imply that charge dissipation of surface charges in pores occurs when measured using a low resistance measurement system.[32,33]

Under short-circuit conditions, the negative charges on PDMS inside pores induce positive charges on the top electrode, while the positive charges on Au NPs induce negative charges on the bottom electrode, and thus electrons in the top electrode move to the bottom electrode through an external circuit to neutralize the positive triboelectric charges in the top electrode, reaching an electrostatic equilibrium due to the electrostatic induction and the conservation of charges, generating a negative current signal. When the top electrode fully reverts to the initial position, there is no electron flow through the circuit. Once the AMTENG is pressed again, the Au NPs will contact with PDMS again, causing the charges to disappear. As a consequence, electrons are driven from the bottom electrode back to the top electrode, reducing the amount of induced charges. This process corresponds to a positive current signal. Au NPs and the PDMS inside the pores are in contact again and all induced charges are neutralized as shown in Fig. 2c.

The electrical output performance also increases almost linearly with the active area (Fig. S6, ESI†). Additionally, and the electrical output performance does not appear to change significantly during 360 s, showing that this AMTENG is proven to be valuable in the reliable design for large-scale production (Fig. 3a and b). To investigate the output power of the AMTENG, resistors were used as external loads from 10 Ω to 1 GΩ, the instantaneous power of the external resistance for the AMTENG reaches a peak value of 6 mW (78 μW cm^{-2}) at a resistance of 10 MΩ, as shown in Fig. 3c and d.

The pores in the mesoporous film play a very important role in determining the electrical output performance of the AMTENG. In detail, the output voltage and current density produced by the nanogenerator at a fixed Au content (0.28 wt%) show that as the porosity increases to 59%, the electrical output performance is significantly enhanced, as shown in Fig. 4a and b. Previously, we showed that one could obtain a higher output performance in a sponge-structured nanogenerator, compared with the flat film, due to the rapid increase of the dielectric constant under the same mechanical force.[29] Actually, as the applied force increases from 0 to 70 mN, the mesoporous film shows a more rapid increase in capacitance, compared with that of the flat PDMS film (Fig. 4c). It is also clearly seen that the rate of the capacitance increases with the porosity. Furthermore, the dramatic increase in the output signals of the nanogenerator can be also attributed to the increase of the surface area-to-volume ratio in the mesoporous PDMS films. The ratio is increased up to several hundred times, as the porosity increases to 59%. Therefore, the contact area is increased by increasing the porosity, increasing the surface charges during the contact of the films, and enhancing the total output power of the nanogenerator (Fig. 4d).

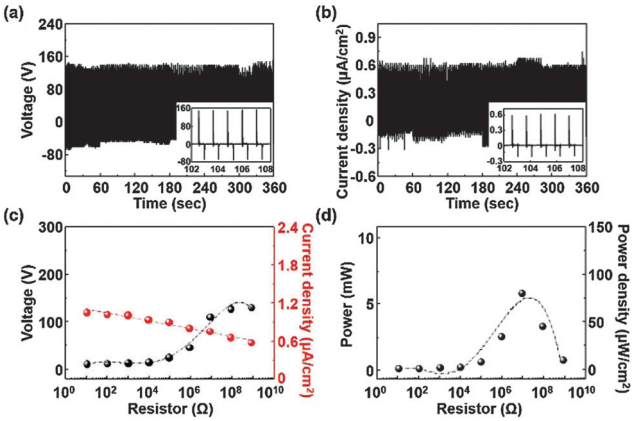

Fig. 3 The output voltage (a) and output current density (b) of the AMTENG under an external force during 360 s. The detailed output voltage and current density of the device are also show in the inset. (c) The output voltage and current density, and (d) the output power of the AMTENG without the gap with the resistance of external loads from 10 to 10^9 Ω.

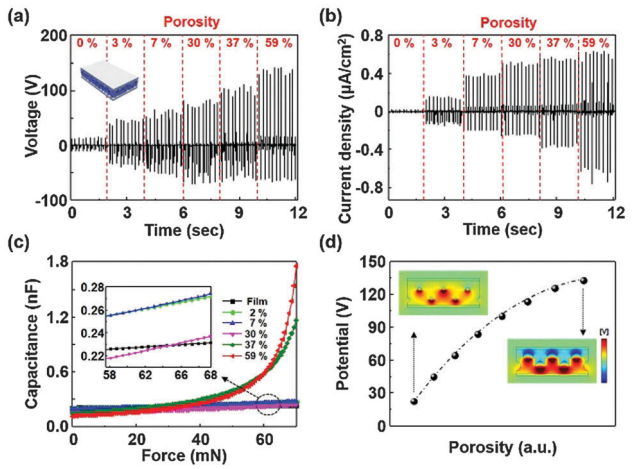

Fig. 4 (a) The output voltage and (b) current density, generated by the AMTENG as a function of the porosity ranging from 0 to 59% at a fixed Au content (0.28 wt%). (c) Force-response capacitance curves for flat films and mesoporous PDMS films with various porosities under external forces from 0 to 70 mN. The detailed capacitance from 0 to 30% porosity is also shown in the inset. (d) The calculated electrostatic potentials of the AMTENG with the increase of porosity simulated using the COMSOL multi-physics software. The inset shows potential distributions in pores of mesoporous films.

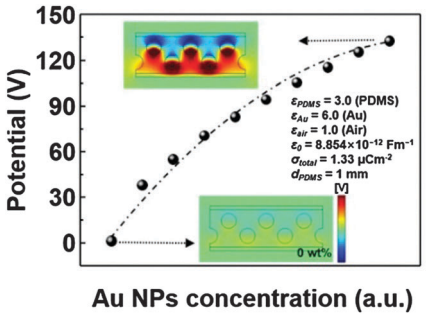

Fig. 5 The calculated electrostatic potentials of the AMTENG with the increase of the Au NP concentration simulated using the COMSOL multi-physics software. The inset show potential distributions in pores of mesoporous film.

On the basis of the above results, the increase in the electrical output performance with increasing Au contents may be understood by the increase in the transferred charge density on the surface of the Au NPs and PDMS inside the pores, as shown in the COMSOL simulations in Fig. 5. The pores in the mesoporous film can be assumed as airgaps in conventional TENGs, in which the devices consist of the Al metal (top electrode)/PDMS/airgap/Au NPs/PDMS/Al metal (bottom electrode), as shown in the ESI,† Fig. S7. When the TENG is fully released, if we assume the electric potential (U_{bottom}) of the surfaces of the bottom PDMS layer to be zero, the electric potential of the surfaces of the top PDMS layer (U_{top}) can be expressed by $U_{top} = \sigma d_{gap}/\varepsilon_0$, where σ is the triboelectric charge density, ε_0 is the vacuum permittivity of free space (8.854×10^{-12} F m^{-1}), and the gap distance (d_{gap}) of the TENG can be calculated as d_{gap} = 476 μm. Thus, the calculated surface charge density (σ) on the surfaces of the top PDMS layer can be obtained by $\sigma = \varepsilon_0 V/d_{gap}$ = 2.79 μC m^{-2}, in which V is the output voltage of our generator (150 V), as shown in Fig. 2a. The maximum surface charge density (σ_{max}') accumulated on the top electrode can be expressed as below[34]

$$\sigma_{max}' = \frac{\sigma d_{gap}^2 \varepsilon_{PDMS} \varepsilon_{Au}}{d_T \varepsilon_{Au} \varepsilon_{PDMS} + d_{gap} \varepsilon_{Au}^2 \varepsilon_{PDMS} + d_{Au}^2 \varepsilon_{PDMS} + d_B \varepsilon_{PDMS} \varepsilon_{Au}} \quad (1)$$

where ε_{PDMS} and ε_{Au} are the relative permittivity of PDMS (3) and Au (6.9), respectively, d_T, d_B, and d_{Au} are the thickness of top and bottom PDMS films (d_T or d_B = ($d_{total} - d_{gap}$)/2 = 262 μm), and Au NPs, respectively. Therefore, one obtains a maximum surface charge density on the top electrode of the TENG of 1.80 μC m^{-2}. The σ_{max}' can be determined by the gap distance d_{gap} defined by the average diameter d_{ave} of pores of the AMTENG, because d_T, d_B, d_{Au}, ε_{PDMS} and ε_{Au} are constants. Thus, since the maximum value of σ_{max}' can be obtained at the maximum of d_{gap} using the above equation, the large porosity of mesoporous films can generate large surface charge density, resulting in the increase of output performance of the AMTENG.

This simple design without the gap enables the sealing process in the device, at the edges of the AMTENG as well as the surface of top and bottom electrodes. The electrical output voltage and current density were measured and are plotted in

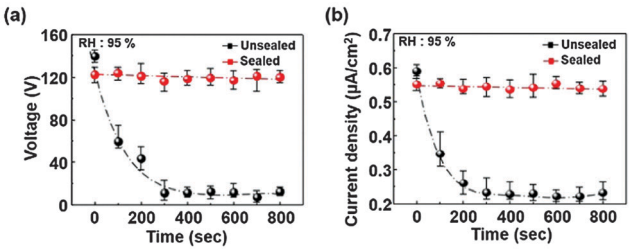

Fig. 6 The change in (a) output voltage and (b) current density of the unsealed and sealed AMTENGs at a relative humidity of 95% RH.

Fig. 6a and b, respectively. It is clearly seen that the rates of the decrease in the output voltage and current density are significantly reduced by sealing. Without the sealing process, the output current density drop rapidly about 85% within 10 min at 95% RH, while there is no significant decrease in the electrical output performance of the sealed film. This results show that the AMTENG can enhance the performance of the generators, less-sensitive to humidity in surroundings, indicating that it is quite stable under harsh environments such as high humidity and even in water.

The bottom electrode was then detached from the mesoporous film and an airgap of 1 mm thickness, made by insulating the polymer with double-sided adhesive, was stacked on the electrode. The above measurement was repeated, as shown in Fig. 7a and b. It is obvious that the output voltage and current density reaches a record value of 220 V and 2 μA cm^{-2} for the AMTENG, in which the output performance of the TENGs also increases with the Au contents. The enhancement of the electrical output performance may be attributed to the relative change in the surface potential level of the PDMS film and the bottom electrode. As mentioned above, a potential difference is produced between the Au NPs and PDMS inside the pores by the contact due to different triboelectric tendencies. This produces a net electric field along the direction from the PDMS to the top electrode, that is, the positive charges are in contact with the bottom electrode, as shown in Fig. 7c. This increases the potential difference with the Fermi level of the bottom electrode. The transferred charge density (σ) on the PDMS surface is defined as

$$\sigma = \frac{[(W - E_0)/e](1 + t/\varepsilon z)}{t/\varepsilon\varepsilon_0 + \left(1/\overline{N_s(E)}e^2\right)(1 + t/\varepsilon z)} \quad (2)$$

where $W - E_0$ is the difference in the effective work functions between two materials, e, t, ε, ε_0, z, and $\overline{N_s(E)}$ are the charge of an electron, distance of space, relative permittivity of PDMS, vacuum permittivity of free space, depth of the mesoporous film, and the averaged surface density of states.[30] Thus, the probability of the charge transfer and the surface charge density increase due to the induced electric field,[35] as shown in Fig. 7d. In addition, we can obtain a calculated surface charge density of 1.95 μC m^{-2} for AMTENG with an airgap of 1 mm at an Au NP content of 0.28 wt%, compared to 5.6 times higher than 0.35 μC m^{-2} of the FTENG. The measured charge density is 2.5 μC m^{-2} under an external force of 90 N and is slightly

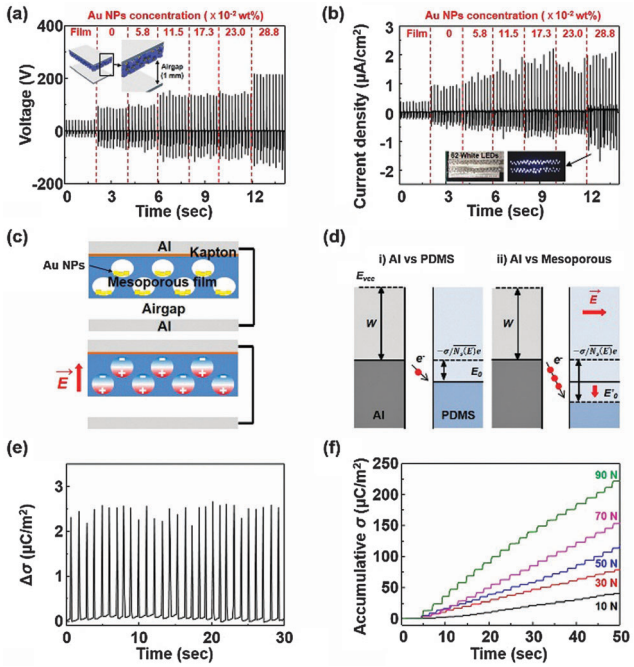

Fig. 7 (a) The output voltage and (b) current density, generated by the AMTENG a specific space of 1 mm as a function of the Au NP concentration ranging from 5.8 to 28.8 $\times 10^{-2}$ wt%. (c) Schematic diagrams of the net electric field in mesoporous films along the direction from PDMS to the top electrode and the contact between positive charges and the bottom electrode. (d) A schematic energy band diagram illustrating the increased probability of the charge transfer and the surface charge density due to the induced electric field. (e) The transferred charge densities ($\Delta\sigma$) and (f) the accumulative charge densities (σ) generated by AMTENGs with a specific airgap of 1 mm under different external forces from 10 N to 90 N.

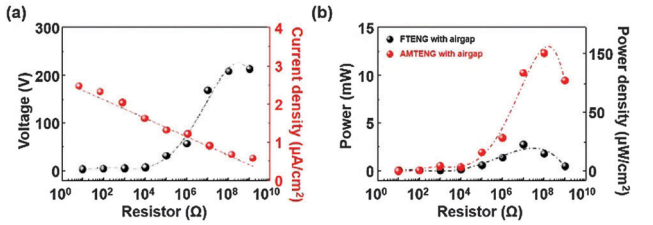

Fig. 8 (a) The output voltage and current density, and (b) the output power of the AMTENG and FTENG with a 1 mm gap with the resistance of external loads from 10 to 10^9 Ω.

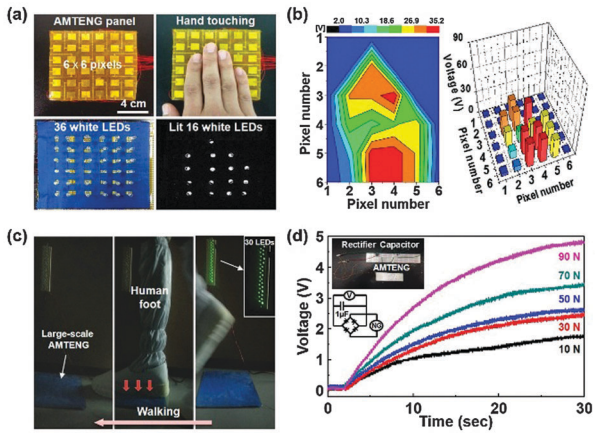

Fig. 9 (a) The self-powered shape mapping sensor with Al electrode arrays (6 × 6) with an area of 1 cm × 1 cm on a mesoporous film. (b) The two-dimensional contour plot and three-dimensional column graph of the peak value of the voltage responses. (c) A large-area AMTENG (30 cm × 30 cm) for harvesting mechanical energy from human walking. (d) The charging process of the capacitor (1 μF) through a full-wave bridge circuit under different external forces from 10 to 90 N.

larger than the calculated one. The difference is attributed to simplifications made in the model and errors that may occur in the measurement. Using a diode bridge to rectify the alternating output signals, the accumulative charge density (accumulative σ) of the AMTENG with an airgap under an external force of 90 N is 225 μC m^{-2} in 50 seconds (Fig. 7e and f).

The output power of the AMTENG was also measured with external loads from 10 Ω to 1 GΩ, as shown in Fig. 8a. It is clearly seen that the output current density drops with the increasing resistance, while the output voltage follows an increasing trend. Consequently, the instantaneous power of the external resistance is 13 mW (160 μW cm^{-2}) at a resistance of 10^7–10^8 Ω, as shown in Fig. 8b, 2 times enhancement in the FTENG with a 1 mm airgap. To verify the ability for powering the electronic devices, we also measured the rectified power of the nanogenerator. The rectified powers are 3 mW (37 μW cm^{-2}) and 8 mW (95 μW cm^{-2}) for the AMTENG without and with an airgap, respectively (Fig. S8, ESI†).

We also demonstrate the self-powered shape mapping sensor for monitoring the local touching actions of the human hand. Al electrode arrays (6 × 6) with an area of 1 cm × 1 cm were fabricated on a single mesoporous film and are connected to the 36 white LEDs, completely covered by a polyimide tape as the sensitive unit to be touched, as shown in Fig. 9a. It is clearly seen that 16 white LEDs in a hand shape can be lit up by hand touching. Fig. 9b shows a two-dimensional contour plot and a three-dimensional column graph of the peak value of the voltage responses, respectively. These plots elaborate the spatial resolution of the bulk mesoporous matrix for distinguishably mapping the calligraphy of the applied pressure, and its potential applications such as shape matching and object recognition. We also fabricate a large-scale AMTENG (30 cm × 30 cm) for harvesting mechanical energy from human walking. It is clearly seen that 30 green LEDs can be lit up by the human foot during walking as shown in Fig. 9c. Although the motion of the human foot is not a perfectly flat, it still can be effectively harvested by the AMTENG. Moreover, because it is available for the large-scale fabrication, the large-scale AMTENG can harvest the walking energy from anyone who steps on the pads. Such a device design can be extended to the square and the subway. Finally, the AMTENG was connected to a capacitor (1 μF) through a full-wave bridge circuit, as shown by the equivalent circuit in the inset of Fig. 9d to demonstrate the application potential as a direct current (DC) power source. Fig. 9d shows the charging process of the capacitor, measured under cycled compressive forces from 10 to 90 N at an applied frequency of 5 Hz using a pushing tester (Labworks Inc., model no. ET-126-4). Higher force yielded higher

saturation voltage of the capacitor, which is a result of equilibrium established the charging and capacitor leakage rates for the AMTENG. The voltage held by the capacitor reached 4.9 V in 30 s under an external force of 90 N.

4. Conclusions

In conclusion, we have demonstrated a facile and scalable synthesis of mesoporous films impregnated with Au NPs as effective dielectrics for enhancing the TENG performance based on a vertical contact-separation mode. The Au NPs were found to be accumulated on one side-wall inside each pore by casting a mixture of the PDMS solution and DI water. The porosity of mesoporous films increases up to approximately 59% as the amount of water increases to 50%. Thus, the mesoporous films were found to be more flexible than the flat films. Our nanogenerator showed an instantaneous power of 13 mW under cycled compressive force, giving over 5-fold power enhancement, compared with a flat film-based TENG, under the same mechanical force. It is believed that the enhancement ascribes to the increase of the density of charges created by the contact between Au NPs and PDMS inside the pores, thereby, influencing the surface potential energy of mesoporous films. The nanogenerator with the mesoporous films was successfully demonstrated in applications for self-powered shape mapping sensors, foot-step driven large-scale AMTENGs, and integrated circuits with capacitors for powering commercial cell phones. This approach provides a promising large-scale power supply for realizing self-powered systems from footsteps, wind power, and ocean waves.

Acknowledgements

This work was supported by Samsung Research Funding Center of Samsung Electronics under Project Number SRFC-TA1403-06.

Notes and references

1 Z. L. Wang and J. H. Song, *Science*, 2006, **312**, 242.
2 X. D. Wang, J. H. Song, J. Liu and Z. L. Wang, *Science*, 2007, **316**, 102.
3 Y. Qin, X. D. Wang and Z. L. Wang, *Nature*, 2008, **451**, 809.
4 R. S. Yang, Y. Qin, L. M. Dai and Z. L. Wang, *Nat. Nanotechnol.*, 2009, **4**, 34.
5 M.-Y. Choi, D. Choi, M.-J. Jin, I. Kim, S.-H. Kim, J.-Y. Choi, S. Y. Lee, J. M. Kim and S.-W. Kim, *Adv. Mater.*, 2009, **21**, 2185.
6 F.-R. Fan, Z.-Q. Tian and Z. L. Wang, *Nano Energy*, 2012, **1**, 328.
7 F.-R. Fan, L. Lin, G. Zhu, W. Wu, R. Zhang and Z. L. Wang, *Nano Lett.*, 2012, **12**, 3109.
8 S. Wang, L. Lin and Z. L. Wang, *Nano Lett.*, 2012, **12**, 6339.
9 G. Zhu, Z.-H. Lin, Q. Jing, P. Bai, C. Pan, Y. Yang, Y. Zhou and Z. L. Wang, *Nano Lett.*, 2013, **13**, 847.
10 S. Wang, L. Lin, Y. Xie, Q. Jing, S. Niu and Z. L. Wang, *Nano Lett.*, 2013, **13**, 2226.
11 L. Lin, S. Wang, Y. Xie, Q. Jing, S. Niu, Y. Hu and Z. L. Wang, *Nano Lett.*, 2013, **13**, 2916.
12 P. Bai, G. Zhu, Y. Liu, J. Chen, Q. Jing, W. Yang, J. Ma, G. Zhang and Z. L. Wang, *ACS Nano*, 2013, **7**, 6361.
13 J. Chen, G. Zhu, W. Yang, Q. Jing, P. Bai, Y. Yang, T.-C. Hou and Z. L. Wang, *Adv. Mater.*, 2013, **25**, 6094.
14 S. Niu, Y. Liu, S. Wang, L. Lin, Y. S. Zhou, Y. Hu and Z. L. Wang, *Adv. Mater.*, 2013, **25**, 6184.
15 Y. Yang, Y. S. Zhou, H. Zhang, Y. Liu, S. Lee and Z. L. Wang, *Adv. Mater.*, 2013, **25**, 6594.
16 H. Zhang, Y. Yang, Y. Su, J. Chen, K. Adams, S. Lee, C. Hu and Z. L. Wang, *Adv. Funct. Mater.*, 2014, **24**, 1401.
17 Y. Yang, H. Zhang, R. Liu, X. Wen, T.-C. Hou and Z. L. Wang, *Adv. Energy Mater.*, 2013, **3**, 1563.
18 P. Bai, G. Zhu, Z.-H. Lin, Q. Jing, J. Chen, G. Zhang, J. Ma and Z. L. Wang, *ACS Nano*, 2013, **7**, 3713.
19 W. Yang, J. Chen, G. Zhu, J. Yang, P. Bai, Y. Su, Q. Jing, X. Cao and Z. L. Wang, *ACS Nano*, 2013, **7**, 11317.
20 Y. Yang, H. Zhang, Z.-H. Lin, Y. S. Zhou, Q. Jing, Y. Su, J. Yang, J. Chen, C. Hu and Z. L. Wang, *ACS Nano*, 2013, **7**, 9213.
21 X. Chen, M. Iwamoto, Z. Shi, L. Zhang and Z. L. Wang, *Adv. Funct. Mater.*, 2015, **25**, 739.
22 Y. Su, X. Wen, G. Zhua, J. Yang, J. Chen, P. Bai, Z. Wu, Y. Jiang and Z. L. Wang, *Nano Energy*, 2014, **9**, 186.
23 G. Zhu, C. Pan, W. Guo, C.-Y. Chen, Y. Zhou, R. Yu and Z. L. Wang, *Nano Lett.*, 2012, **12**, 4960.
24 Y. S. Zhou, Y. Liu, G. Zhu, Z.-H. Lin, C. Pan, Q. Jing and Z. L. Wang, *Nano Lett.*, 2013, **13**, 2771.
25 E. d. Wolf, G. v. Koten and B.-J. Deelman, *Chem. Soc. Rev.*, 1999, **28**, 37.
26 V. K. Agarwala and T. Fort, *Surf. Sci.*, 1974, **45**, 470.
27 F. R. Fan, J. Luo, W. Tang, C. Li, C. Zhang, Z. Tian and Z. L. Wang, *J. Mater. Chem. A*, 2014, **2**, 13219.
28 Y. Yang, H. Zhang, J. Chen, S. Lee, T.-C. Houa and Z. L. Wang, *Energy Environ. Sci.*, 2013, **6**, 1744.
29 K. Y. Lee, J. Chun, J.-H. Lee, K. N. Kim, N.-R. Kang, J.-Y. Kim, M. H. Kim, K.-S. Shin, M. K. Gupta, J. M. Baik and S.-W. Kim, *Adv. Mater.*, 2014, **26**, 5037.
30 Y. S. Zhou, S. Wang, Y. Yang, G. Zhu, S. Niu, Z.-H. Lin, Y. Liu and Z. L. Wang, *Nano Lett.*, 2014, **14**, 1567.
31 J.-T. Zhang, L. Wang, D. N. Lamont, S. S. Velankar and S. A. Asher, *Angew. Chem., Int. Ed.*, 2012, **51**, 6117.
32 I. P. Seshadri and B. Bhushan, *J. Colloid Interface Sci.*, 2008, **325**, 580.
33 A. R. Blythe, *Polym. Test.*, 1984, **4**, 195.
34 Z.-H. Lin, G. Cheng, Y. Yang, Y. S. Zhou, S. Lee and Z. L. Wang, *Adv. Funct. Mater.*, 2014, **24**, 2810.
35 P. Bai, G. Zhu, Y. S. Zhou, S. Wang, J. Ma, G. Zhang and Z. L. Wang, *Nano Res.*, 2014, **7**, 990.